

# Beam-Riding of a Parabolic Laser Lightcraft

**S. Scharring<sup>a</sup>, H.-A. Eckel<sup>a</sup> and H.-P. Röser<sup>b</sup>**

<sup>a</sup>Institute of Technical Physics, German Aerospace Center (DLR), Stuttgart, Germany

<sup>b</sup>Institute of Space Systems, University of Stuttgart, Germany

## Abstract

The impulse coupling characteristics of a parabolic laser-driven thruster ('lightcraft') are investigated in free flight experiments using a pulsed CO<sub>2</sub> high energy laser. The analysis of 3D high speed recordings reveals lateral force components as well as angular momentum re-orientating the lightcraft towards the laser beam in the case of slight misalignment. Beam-riding properties are examined with respect to the initial lateral offset at the launch position revealing a strong interdependency of lateral and angular motion. The experimental results are compared with model data derived from raytracing analysis of the fluence distribution on the surface of an ignition pin which is located on the lightcraft's symmetry axis. Based on model data, beam-riding abilities are characterized with respect to initial offset and inclination by means of Julia sets. The parameter space of tolerable misalignment is explored with respect to laser burst parameters and compared with experimental data.

## 1. INTRODUCTION

Soon after the invention of laser, thrust generation by laser ablation was reported by [1]. The vision of a remote energy supply for an aerospace vehicle by a directed laser beam was initially formulated by Arthur Kantrowitz [2]. Among the various laser propulsion concepts, pulsed laser propulsion based on laser ablation and laser supported detonation attracted great interest, since the issue of beam-riding was clearly addressed in the free flights up to the world record altitude of 71 m achieved by the group of Leik Myrabo [3,4]. Since remote propulsion enables a significantly improved mass-to-payload ratio compared to conventional space rockets, it may represent a cost-effective propulsion alternative for the launch of small satellites from ground to orbit, once a powerful laser with appropriate beam-guiding facilities is installed [5]. At present, the development of high energy lasers with an adequate average power appears to be the bottleneck of this technology [6]. This limitation actually shifts the scope of interest to applications in microgravity; e.g., in-space remote propulsion [7], attitude control by on-board micropropulsion [8], and space debris removal [9].

Nevertheless, the great potential of beamed energy propulsion demands for a thorough investigation of the beam-riding technology with respect to various thruster configurations. For demonstration purposes, spin stabilization may be applicable. However, it might diminish the steering potential of the thruster in the further course of a prospective mission. Hence, detailed studies on lateral and angular impulse components are reported for the lightcraft technology demonstrator (LTD) of Myrabo [10,11,12]. The LTD exhibits a focusing geometry of an inverted parabola with an outer focal ring, where a propellant torus of Delrin<sup>®</sup> (polyoxymethylene, POM) is placed. In contrast, the type of lightcraft used in the experiments at DLR exhibits a parabolic shape with either a cylindrical propellant rod on the axis of symmetry or an ignition pin. The latter device provides for a reproducible ignition at the focus [13,14]. Thrust generation of both lightcraft types was compared in earlier studies [15]. This paper presents experimental results and model calculations on the lateral and angular components of a parabolic lightcraft with respect to beam-riding abilities.

## 2. EXPERIMENTAL SETUP

### 2.1. Laser source

In our experiments, an electron-beam sustained CO<sub>2</sub> high energy laser was employed as a remote energy source for the propulsion of the laser-driven lightcraft. The laser pulse energies in a stable resonator configuration are in the range of 30 to 200 J, with pulse duration around 10 μs, depending on the laser pulse energy. The laser was operated in repetitive mode with burst repetition rates up to 50 Hz. Laser burst parameters are mainly limited by the actual power supply which provides for a maximum average optical laser power of 15 kW at an electro-optical efficiency of around 10%. The laser system is characterized in detail in [16], data from recent measurements are found as well in [17].

The laser beam exhibits an elliptical shape with a horizontal diameter of around 80 mm, a little less in vertical direction. Through a small aperture in the center of the rear mirror of the resonating cavity, a HeNe laser is passed coaxially with the CO<sub>2</sub> beam direction for alignment purposes. During the laser burst, however, the HeNe laser beam is blocked by a pyrodetector for measurement of the laser pulse energy that escapes through the small aperture at the rear side of the CO<sub>2</sub> laser. This technique allows for real-time monitoring of the pulse energy, since the recorded data are proportional to the laser pulse energy directed to the lightcraft via the ZnSe output coupler of the laser cavity.

### 2.2. Lightcraft

The lightcraft mainly consists of a parabolic mirror made from aluminum. It combines two features of the propulsion process, since it both focuses the incoming light and acts as a nozzle for the expanding gas. During a laser pulse, the laser light intensity in the focal zone exceeds the threshold of air breakdown. Hence, a laser-supported detonation wave is raised. The exhaust of the hot gas leads to a momentum that is imparted to the thruster. Its magnitude strongly depends on aperture diameter, focal length, pulse energy and ambient pressure [18]. In our experiments, the lightcraft exhibited an aperture diameter of 100 mm, a focal length of 10 mm, and an overall height of 62.5 mm. In order to enhance the reproducibility of the propulsion process, a metallic ignition pin lowering the ignition threshold was used on the axis of symmetry of the lightcraft.

A lightweight cap of polyamide made by laser-sintering was attached to the thin reflector (0.5 mm wall thickness) to prevent it from damage at touchdown after the free flights. Furthermore, a huge net was stretched around the launchpad.

### 2.3. Free flight test range

We placed the lightcraft on a launchpad consisting of three steel rods in a 120° configuration. This construction was intended to avoid ground effects [19]. Below the launchpad, a planar mirror made of copper was adjusted to direct the laser beam into the vertical. For alignment of the launch position of the lightcraft, a pinhole was placed between the output coupler of the laser and the bending mirror. Inclination of the launchpad was controlled by back-reflection of the part of the HeNe laser beam that passed the pinhole from a planar mirror placed on the launchpad instead of the lightcraft. Lateral offset of the lightcraft was subsequently adjusted by variation of the pinhole position inside the HeNe laser spot and alignment of the lightcraft center – indicated by the pin – according to the transmitted HeNe ray.

The laser pulse energy was measured with a pyrodetector (Ophir Electronics Ltd., PE 50-BB) connected to a control unit (Ophir Electronics Ltd., Laserstar Dual Channel). The flight path of the lightcraft was recorded with a high speed camera (Redlake, MotionScope M3) set at a temporal resolution of 500 fps. For the reconstruction of the 3D trajectory, an additional mirror was placed next to the flight path at an angle of 45° to record a side view of the movement simultaneously. The effect of the laser pulses can easily be spotted in the high speed frames due to plasma recombination light. This allows for a precise determination of the flight segments and for the analysis of the corresponding impulse coupling coefficients.

### 2.4. Data analysis and modeling

Image acquisition software (AOS Technologies AG, Imaging Studio V2.2.0.6) was used to sample the high speed videos for subsequent tracking with an image processing software (IDTvision, MotionPro X 2.04.03). Four markers each were used for tracking the lightcraft's position in the *x-z*-plane as well as in the *y-z*-plane.

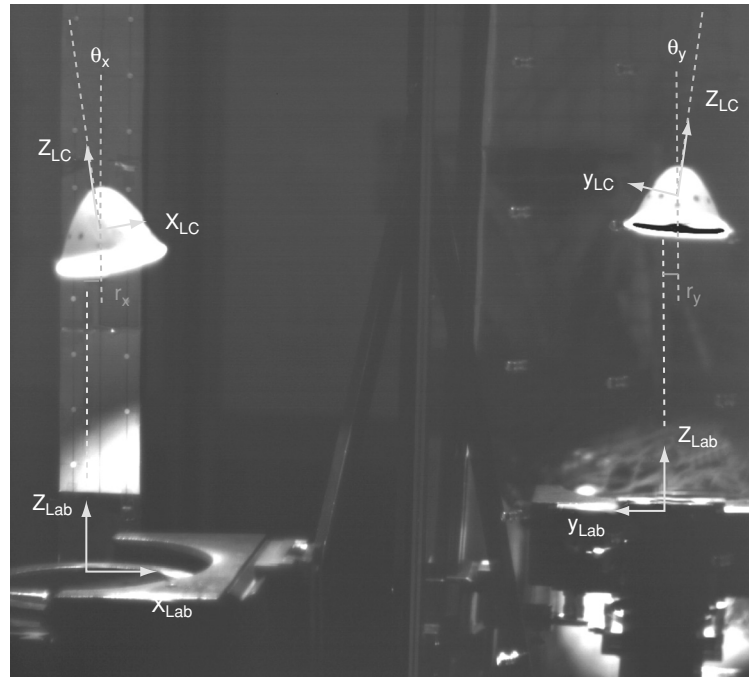


Figure 1. Test range for free flight experiments with a laser-driven thruster. This frame is taken from a high speed recording and shows recombination light from laser induced plasma. The laboratory system is denoted with an index 'Lab', whereas 'LC' refers to the coordinate system of the lightcraft. Inclination angle and lateral offset are indicated with respect to the plane of observation. In this example,  $r_x$ ,  $\theta_x$ ,  $\theta_y$  are positive,  $r_y$  is negative.

Further data processing was carried out with Origin 8.0 and Mathematica 6.0. The data of the flight path were analyzed with respect to the position of the lightcraft's CMS and its inclination to the horizontal plane. This technique is described in [14]. For each segment between laser pulses within a burst, the data for lateral and angular motion were fitted linearly, and quadratically for vertical motion, resp. From the translational and angular velocity increments at the times of the laser pulse, the momentum coupling coefficients were derived corresponding to the direction of translation and rotational axes. Since lateral and angular motion are quite small compared to the whole flight range in  $z$ -direction, corresponding tracking data show a large scatter. Hence, artifacts from tracking and datafits with poor correlation were excluded from further analysis.

The fluence distributions on the surface of the ignition pin were modeled with a raytracing software (Wolfram Research, Optica 3.0). Details on this calculation are given in [20].

### 3. FLIGHT EXPERIMENTS

The beam-riding properties of the lightcraft were investigated by varying its alignment against the beam center at the launch position before the flight within a range of  $\pm 5$  mm. Pulsed free flights with a lightcraft of a mass  $m_{LC} = 53.8$  g have been carried out with a laser burst consisting of 10 pulses. For technical reasons, the pulse energy for a reliable laser burst without any arc discharges in the laser cavity was limited at the upper end leading to  $E_L = (139 \pm 7)$  J. It can be seen from Equation 2 and Table 1 that this selection requires an average laser power of at least 3.2 kW for a positive thrust. Hence, we chose  $f_{rep} = (36.1 \pm 0.5)$  Hz (5 kW average laser power) in order to obtain a large flight range with detailed observation possibilities.

#### 3.1. Flight altitude

The impulse coupling coefficient  $c_m$  is commonly used as a figure of merit for characterization of laser propelled devices. It is defined by the ratio of imparted momentum  $p$  vs. laser pulse energy  $E$ . In the case of a multiple pulsed flight during a laser burst, it can be characterized as well by the ratio of average thrust  $T$  vs. average laser power  $P$ :

**Table 1. Effective coupling coefficient and averaged coupling coefficient for 10 subsequent pulses and variation of the initial offset of the lightcraft against the laser beam.**

Initial offset [mm]	Average acceleration [m/s <sup>2</sup> ]	$c_{m,eff}$ [N/MW]	$c_m$ [N/MW]
-5	$3.87 \pm 0.37$	$41.5 \pm 4.5$	$146.7 \pm 17.7$
-3	$4.74 \pm 0.27$	$50.8 \pm 3.9$	$156.0 \pm 14.5$
-1	$5.19 \pm 0.33$	$55.7 \pm 4.6$	$160.9 \pm 15.7$
0	$5.64 \pm 0.19$	$60.5 \pm 3.8$	$165.7 \pm 13.5$
+1	$5.41 \pm 0.73$	$58.0 \pm 8.4$	$163.2 \pm 25.0$
+3	$5.12 \pm 0.47$	$54.9 \pm 5.8$	$160.1 \pm 18.8$
+5	$4.45 \pm 0.42$	$47.7 \pm 5.1$	$152.9 \pm 18.2$

$$c_m = \frac{p}{E} = \frac{T}{P} \quad (1)$$

In the case of a ground based launch, however, thrust is diminished by gravity yielding an effective coupling coefficient  $c_{m,eff}$  [21]:

$$c_{m,eff} = \frac{T - m_{LC} \cdot g}{P} = c_m - \frac{m_{LC} \cdot g}{P} = \frac{R}{P} \quad (2)$$

where  $g$  denotes the gravitational acceleration. In our experiment, we determined  $c_{m,eff}$  with respect to the initial lateral offset  $r_x$  of the lightcraft against the laser beam. We derived the average acceleration with a parabolic fit of the time-altitude curve, cf. Figure 2. We determined  $c_{m,eff}$  by the ratio of accelerating force  $R$  to average laser power  $P$  and derived  $c_m$  according to Equation 2. The results are

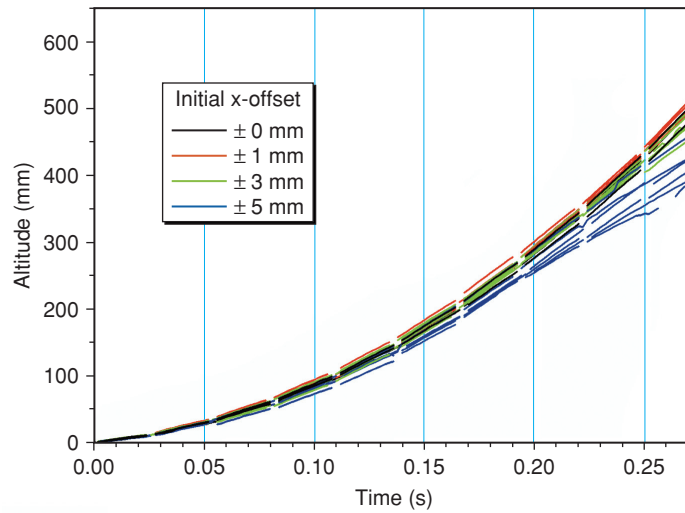


Figure 2. Temporal course of the flight altitude in the acceleration period of laser-driven free flights with the initial offset against the laser beam center as a variable parameter.

shown in Table 1. It turns out that with  $r_x > 2$  mm, momentum coupling into beam axis direction decreases and significantly drops at  $r_x = 5$  mm. In general, even in case of no initial offset the results for  $c_m$  averaging several subsequent pulses in a free flight are considerably lower than results from single pulse experiments, where we measured  $c_m = 306 \pm 5$  N/MW at a comparable pulse energy of  $E = 133$  J [14]. There we already reported a similar trend for averaged values in a flight compared to

single pulse measurements. However, this finding might not be mainly deduced from friction losses. The frictional force was assessed for a maximum speed of  $v_{max} = 5.3$  m/s resulting from 10 pulses at  $f_{rep}$  with optimal momentum coupling yielding only a deceleration of less than 0.5% of  $v_{max}$  during one repetition period. A main reason for thrust reduction during the flights can be found in the decrease of the coupling coefficient with offset and inclination, as it will be discussed later. Moreover, turbulences in the optical path resulting from the hot gas exhaust may also lower the laser fluence inside the lightcraft.

### 3.2. Lateral offset

The initial offset of the lightcraft does not only have an effect on the thrust in the direction of beam propagation. The lateral offset of the lightcraft shows a distinct temporal course that is depicted in Figure 3(a). Varying the offset in y-direction, we found similar results.

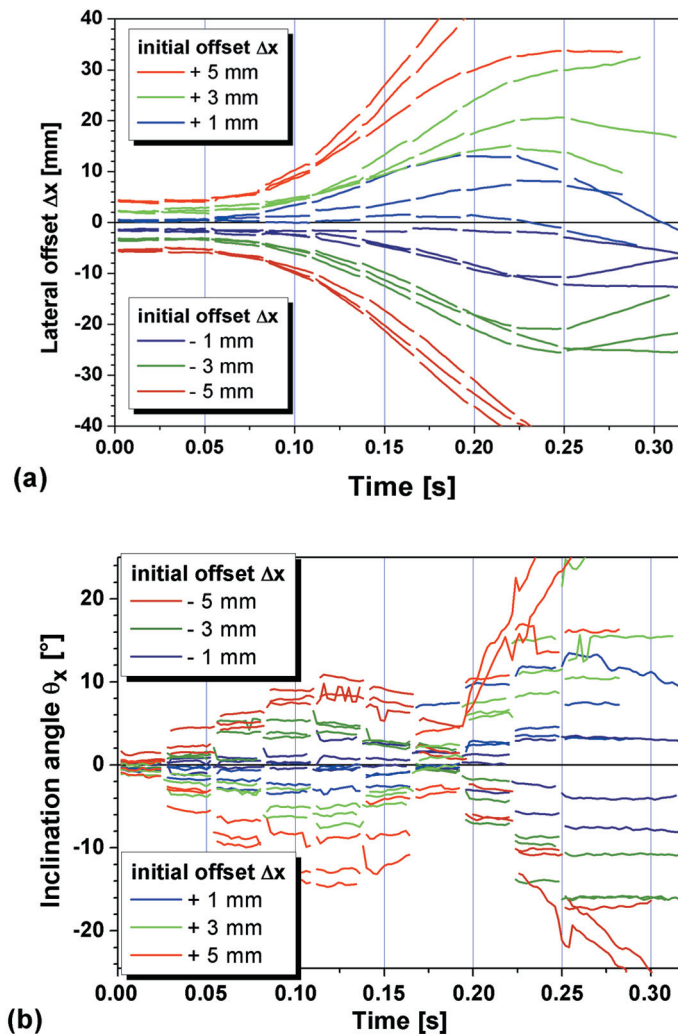


Figure 3. Beam-riding properties of the lightcraft derived from free flight experiments.

For the first seven pulse segments, the offset increases. Then the lightcraft turns back to the beam center again, unless a critical initial offset  $|\Delta_x| \approx 3$  mm is not exceeded. This finding proves the existence of back-driving forces for the parabolic lightcraft. However, the effect of the back-driving force is not seen directly within the first pulses. This may partly be attributed to the fluence distribution on the surface of the ignition pin. With increasing lateral offset, the difference increases between the energy portion deposited on the area directed towards the beam center and the one on the area directed apart from it.

The back-driving force can be quantified by measuring the oscillation period of the lateral movement. We found an equivalent spring constant of  $15.9 \pm 8.3$  mN/mm for the  $x$ -direction and  $22.0 \pm 7.8$  mN/mm for the  $y$ -direction, resp. [20]. In [14], we derived similar results from the properties of arc shaped ground trajectories that indicated an oscillation of the lightcraft around an axis near the beam center. This approach has also been used in [10].

As a main result from comparing the graphs of positive and negative offset, we find that using an ignition pin inside a parabolic lightcraft turns the thruster into a system that is direction sensitive. This finding stands in contrast to the model of a point explosion at the lightcraft focus, where any information on direction vanishes [14].

### 3.3. Inclination angle

The initial inclination angle was set to zero in these experiments. Nevertheless, the inclination of the lightcraft shows a pronounced temporal course as well, cf. Figure 3(b). It exhibits a sinusoidal shape with an amplitude that increases with the absolute value of the initial offset. Again, this behavior is sensitive to the initial offset direction. The temporal course passes zero roughly at the time, when the lightcraft starts turning back to the laser beam center. From the analysis of the oscillation of the inclination angle, we find an equivalent spring constant of  $2.8 \pm 1.6$   $\mu$ Ns/mrad for the  $x$ -direction and  $3.9 \pm 2.1$   $\mu$ Ns/mrad for the  $y$ -direction, resp. However, it should be pointed out that in contrast to a simple mass connected to a spring, this system exhibits discrete interaction times, where an impulse is imparted depending on the initial parameters. Hence, it is probable, that the effectiveness of back-driving forces will strongly depend on the laser repetition rate as well as on the laser pulse energy, cf. Section 5. Furthermore, the range of the back-driving force is limited to the interaction zone with the laser beam.

In addition to that, the comparison of the two graphs suggests examination of the interdependency of offset and inclination angle during a laser propelled flight. The imparted lateral momentum should depend on the inclination angle of the craft and vice versa. In order to understand the complex behavior of this non-linear dynamic system, the corresponding impulse components are investigated in the following section in the 2D parameter space of inclination and offset.

## 4. IMPULSE COMPONENTS

### 4.1. Concept

In contrast to a point explosion at the lightcraft's focus, the employment of an ignition pin provides for spatial information given by the fluence distribution. Hence, the lightcraft's position relative to the laser beam should directly affect the resulting force components. In [20], we derived the force components of the laser supported detonation originating from the surface of an ignition pin on the axis of symmetry of a parabolic thruster.

We examine an infinitesimal segment  $dA_p = r_p \cdot d\varphi \cdot dz$  on the surface of the ignition pin, where  $r_p$  is the radius of the ignition pin,  $r_p = 1$  mm in our case, and  $\varphi, z$  denote the corresponding cylindrical coordinates. Then the laser pulse energy  $E$  can be written as

$$E = \iint \Phi(\varphi, z) r_p d\varphi dz \quad (3)$$

Furthermore, we look at an infinitesimal segment  $dA_{LC} = r_{LC} \cdot d\varphi \cdot dz$  on the surface of the lightcraft's wall. Then the imparted momentum  $p$  can be written as

$$p = \iint p(\varphi, z) d\varphi \cdot r_{LC}(z) \sqrt{1 + (\partial_z r_{LC}(z))^2} dz \quad (4)$$

where  $r_{LC}(z)$  is given by the lightcraft's shape, in our case:

$$r(z) = \sqrt{40z} \quad (5)$$

with  $z$  ranging from 0 mm to 62.5 mm. We carry out the integration over  $z$  yielding the following definitions:

$$\Phi^{(\varphi)} = \int \Phi(\varphi, z) r_p dz,$$

$$p^{(\varphi)} = \int p(\varphi, z) r_{LC}(z) \sqrt{1 + \left( \frac{\partial r_{LC}}{\partial z}(z) \right)^2} dz, \quad (6)$$

At first, in the case of perfect alignment of the lightcraft to the laser beam we obtain

$$\partial_\varphi \Phi^{(\varphi)} = \partial_\varphi p_z^{(\varphi)} \equiv 0 \rightarrow p_z^{(\varphi)} = c_m \cdot \Phi^{(\varphi)} \quad (7)$$

which can be deduced for the  $z$ -direction from the definition of  $c_m$ . In the following, our model approach is to generalize Equation 7 for the case of lateral offset and / or tilt of the lightcraft

$$p^{(\varphi)} = c_m (2\pi \cdot \Phi^{(\varphi)}) \cdot \Phi^{(\varphi)} \quad (8)$$

with

$$c_{m,z}(2\pi \cdot \Phi^{(\varphi)}) = c_m(E(\varphi)) \quad (9)$$

where  $E(\varphi)$  denotes the laser pulse energy that is equivalent to the angular fluence  $\Phi(\varphi)$  on the lightcraft's ignition pin under the angle  $\varphi$ . Lateral and rotational momentum components that would vanish in case of perfect alignment can be deduced from integration of the angular fluence  $\Phi(\varphi)$  for any case of misalignment, cf. Figure 4.

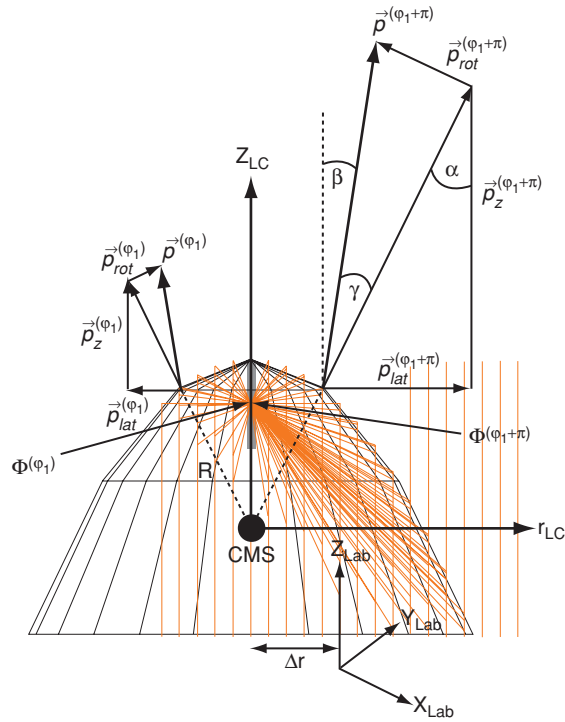


Figure 4. Angular fluence and momentum components for a parabolic lightcraft with a lateral offset  $\Delta r$  against the laser beam center.

Assuming that  $\alpha$ ,  $\beta$ , and  $\gamma$  do not depend on  $\varphi$ , we derive

$$p_z = \int p_z^{(\varphi)} d\varphi \approx \cos \vartheta \int c_m (2\pi \cdot \Phi^{(\varphi)}) \cdot \Phi^{(\varphi)} d\varphi$$

$$p_{lat} = \int p_{lat}^{(\varphi)} d\varphi \approx \tan \alpha \cos \vartheta \int c_m (2\pi \cdot \Phi^{(\varphi)}) \cdot \Phi^{(\varphi)} d\varphi \quad (10)$$

$$p_{rot} = \int p_{rot}^{(\varphi)} d\varphi \approx \tan \gamma \cos \alpha \int c_m (2\pi \cdot \Phi^{(\varphi)}) \cdot \Phi^{(\varphi)} d\varphi$$

where the inclination angle  $\vartheta$  of the lightcraft against the beam propagation axis is given by

$$\tan^2 \vartheta = \tan^2 \vartheta_x + \tan^2 \vartheta_y \quad (11)$$

cf. Figure 1. For simplification, we chose the inclination angle so that it was located in the plane spanned by the direction of lateral offset and beam propagation.

Although in most cases  $c_m(E)$  strongly depends on  $E$ , as found experimentally e.g. in [14,15,17,18,21] and derived theoretically in [14,18], for simplicity reasons  $c_m(E) = const.$  is assumed in the following. Then we finally obtain:

$$\begin{aligned} c_{m,z} &= \frac{\cos \vartheta \cdot c_m}{E} \cdot \int \Phi^{(\phi)} d\phi \\ c_{m,x} &= \frac{P_x}{E} = \frac{c_{lat} \cdot \cos \vartheta \cdot c_m}{E} \cdot \int \Phi^{(\phi)} \cos \phi d\phi \\ c_{m,y} &= \frac{P_y}{E} = \frac{c_{lat} \cdot \cos \vartheta \cdot c_m}{E} \cdot \int \Phi^{(\phi)} \sin \phi d\phi \\ c_{L,x} &= \frac{L_x}{E} = \frac{c_{rot} \cdot c_m}{E} \cdot \int \Phi^{(\phi)} \cos \phi d\phi \\ c_{L,y} &= \frac{L_y}{E} = \frac{c_{rot} \cdot c_m}{E} \cdot \int \Phi^{(\phi)} \sin \phi d\phi \end{aligned} \quad (12)$$

where  $L$  is the rotational momentum and  $c_{lat}$ ,  $c_{rot}$  are constants that will be assessed experimentally in the following. Note that the modeling results in this section will be given in arbitrary units. Hence, if energy losses occur inside the thruster, e.g. from absorption at the reflector walls or from laser-induced plasma, we assume that – in the case of perfect alignment – the magnitude of these losses will not depend on  $\phi$ .

Though we focused our experiments on laser-supported detonation originating from an ignition pin, this model might also be applicable for laser ablative propulsion in the case where the ignition pin is replaced by a propellant rod, e.g. made of POM (Polyoxymethylene, Delrin™). In this case, however, the dependency of  $c_m$  on the laser pulse energy as reported e.g. in [17] should be taken into account.

#### 4.2. Axial momentum

From Equation 12, the impulse coupling coefficient  $c_{m,z}$  in direction of the beam propagation axis can be derived. Its dependency on lateral offset and inclination of the lightcraft was modeled based on the data from raytracing [20]. The results are depicted in Figure 5. Since the focusing properties of the parabolic reflector surface are only affected by the inclination angle, but not by the lateral offset, the impact of inclination on coaxial thrust is much more pronounced.  $C_{m,z}$  already decreases at  $\theta \approx \pm 1^\circ$  while it nearly remains constant for a lateral offset of  $\pm 10$  mm. The latter range can be attributed to the lightcraft's aperture diameter which exceeds the laser beam diameter by  $\sim 20$  mm.

#### 4.3. Lateral momentum

From the raytracing data, we derived the momentum coupling coefficient in the direction lateral to the beam propagation axis. The results are depicted in Figure 6(a). From its distribution, it can be seen, that a back-driving force component occurs exhibiting a maximum at an offset of around 30 mm. However, it is strongly dependent on the inclination angle of the lightcraft. It is most pronounced at an inclination angle of  $1^\circ$  to  $2^\circ$  and  $\text{sgn}(\theta) = -\text{sgn}(r)$ . Though we found a similar trend in the experiments with respect to the offset, cf. Figure 6(b), for the dependency on the inclination angle an opposite behaviour is found. However, it can clearly be confirmed, that an interdependency of lateral and angular motion exists.

From the comparison of the maxima in the modeling (a) and in the experimental results (b), we find as a coarse approximation  $c_{lat} \approx 0.35$ , cf. Equation 12, assuming the value of  $c_m$  from single pulse experiments in [14].

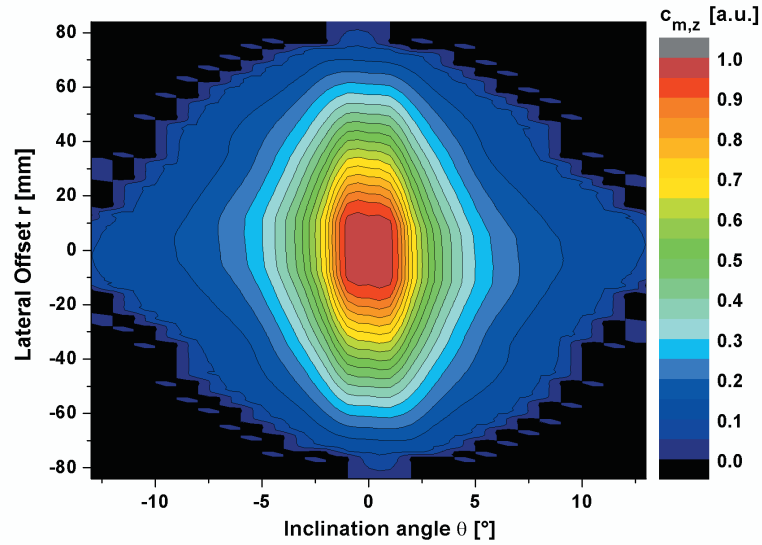


Figure 5. Vertical component  $c_{m,z}$  of the impulse coupling coefficient based on results of raytracing for the surface of the ignition pin inside the lightcraft.

#### 4.4. Rotational momentum

The model data for the rotational momentum, cf. Figure 7(a), show back-driving properties, too. However, the range of this force only covers  $\pm 5^\circ$ . Again, an interdependency on the offset is found that supports the back-driving momentum in the case of  $\text{sgn}(\theta) = -\text{sgn}(r)$ . The dependency on the offset is confirmed by the experimental data, while the dependency on the inclination angle is not clearly visible from the fitting results. This may be attributed to the large field of view of the high speed camera having a detrimental effect on the angular resolution. A similar dependency of lateral and angular impulse on the lateral offset was reported for the LTD of Myrabo in [10, 11].

From the comparison of the maxima in the modeling (a) and in the experimental results (b), we find a rough estimate of  $c_{rot} \approx -1.2 \cdot 10^{-3}$  m, cf. Equation 12.

## 5. FLIGHT PREDICTIONS

### 5.1. Visualization of beam-riding stability as a Julia set

For lateral and rotational momentum back-driving force components have been found that exhibit a non-linear characteristic. Moreover, their impact is restricted to a propulsion process which is limited to several hundreds of microseconds [18], which is relatively short compared to the applied pulse repetition periods that were equal or larger than 20 ms in our experiments. Hence, at the moment of the  $n^{\text{th}}$  laser pulse, magnitude and direction of lateral and rotational momentum strongly depend on the actual lateral offset and inclination of the lightcraft that in turn strongly depend on lateral offset and inclination immediately before the previous pulse as well as on the repetition rate. Since we found in Section 4.3 and 4.4 that offset and inclination affect each other, a simple prediction on the flight stability cannot be made. In contrast, if we combine offset  $r$  and inclination  $\vartheta$  of the lightcraft to a complex number  $z^{(n)} = (r, \vartheta) \in \mathbb{C}$  that indicates the misalignment of the lightcraft immediately before the  $n^{\text{th}}$  pulse, the long-term behaviour of  $z^{(n)}$  ( $n \rightarrow \infty$ ), i.e. the beam-riding ability of the lightcraft, strongly depends on the initial value  $z^{(l)}$ .

Fractals are commonly used to visualize the long-term behavior of a non-linear and possibly chaotic system. Among them, Julia sets are widely known examples. For an arbitrarily chosen polynomial function  $f$  on the complex numbers the corresponding Julia set  $J_f$  is defined as the set of points with orbits that do not converge to the Point at Infinity [22]:

$$J_f = \{z \in \mathbb{C} : \lim_{n \rightarrow \infty} |f^{(n)}(z)| < \infty\}. \quad (13)$$

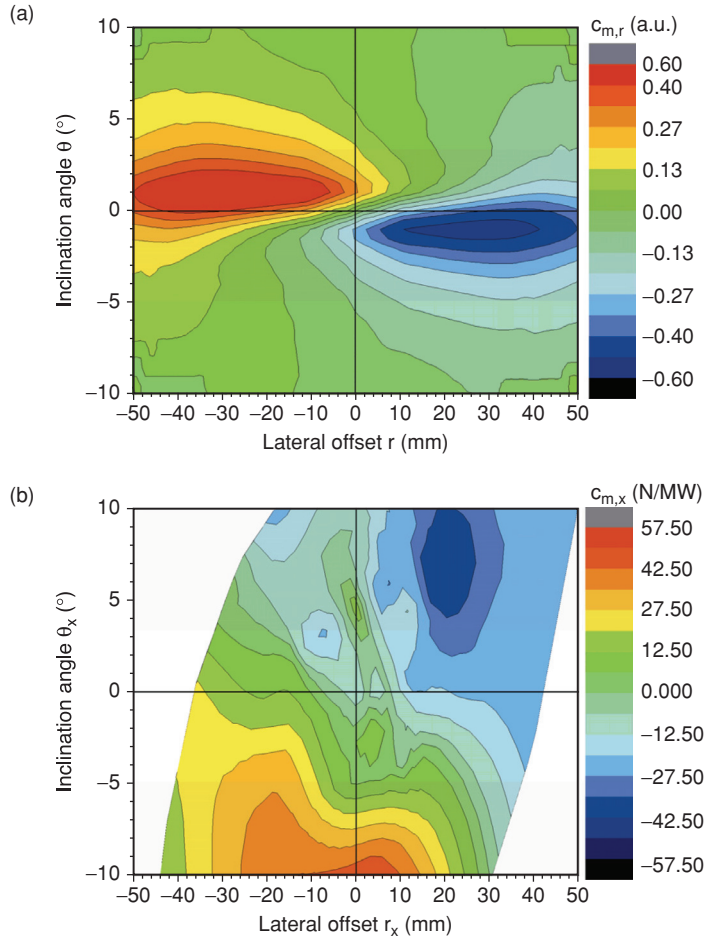


Figure 6. Dependency of the lateral impulse on lateral offset and inclination angle of the lightcraft against the laser beam. Theoretical results from fluence distribution modeling (a) are compared with experimental data (b), cf. Section 3.2.

This concept can be applied to the laser lightcraft as a pulsed non-linear dynamic system. In our case, we define a function  $f: \mathbb{C} \rightarrow \mathbb{C}$  that allows for the calculation of the lightcraft's misalignment  $z^{(n+1)}$  directly before the  $n+1$ st pulse from its misalignment  $z^{(n)}$  according to

$$f : \begin{cases} v_r^{(n+1)} = v_r^{(n)} + \frac{E}{m_{LC}} c_{m,r}(r^{(n)}, \vartheta^{(n)}) \\ \omega^{(n+1)} = \omega^{(n)} + \frac{E}{J_r} c_L(r^{(n)}, \vartheta^{(n)}) \\ r^{(n+1)} = r^{(n)} + v_r^{(n+1)} T_{rep} \\ \vartheta^{(n+1)} = \vartheta^{(n)} + \omega^{(n+1)} T_{rep} \end{cases} \quad (14)$$

where  $v_r$  is the lateral velocity and  $\omega$  the angular velocity of the lightcraft and  $(n)$  indicates position and velocity immediately before the  $n$ th laser pulse. The coupling coefficients  $c_{m,r}$  and  $c_L$  are given by Equation 12. The repetition period of the laser burst is denoted with  $T_{rep}$  and  $J_r$  represents the lightcraft's inertial momentum referring to its rotational axis. Since friction losses are neglected in this approach, this system of equations simply describes the uniform linear lateral motion and rotation for each segment between the laser pulses.

We define the set  $L$  of parameters where thrust is expected to be generated as

$$L = \{z \in \mathbb{R} \mid (c_{m,z}(z) > 0)\}. \quad (15)$$

Rewriting Equation 13, the corresponding Julia set of launch parameters yielding a stabilized flight can be defined as

$$J_f = \{z \in L : \lim_{n \rightarrow \infty} f^{(n)}(z) \in L\}. \quad (16)$$

## 5.2. Julia sets with modified flight parameters

Modeling of the beam-riding stability can be performed by inserting the modeling results based on raytracing for impulse coupling, cf. Equation 12, into the function for misalignment calculation, cf. Equation 14. Since the experimental results for the constants  $c_m$ ,  $c_{lat}$  and  $c_{rot}$  are known, cf. [14] and Section 4, the corresponding Julia sets can be evaluated numerically. Initial launch parameters  $z$  were tested with respect to beam riding abilities applying a grid of  $0.1^\circ$  (inclination) and 0.1 mm (offset) resolution.

The corresponding Julia sets are shown in Figure 8. Each Julia set was calculated for a distinct choice of laser burst parameters that are given in Table 2. For each  $z$ , the calculation of beam riding abilities was stopped if  $n > 100$  or  $z^{(n)} \notin L$ .

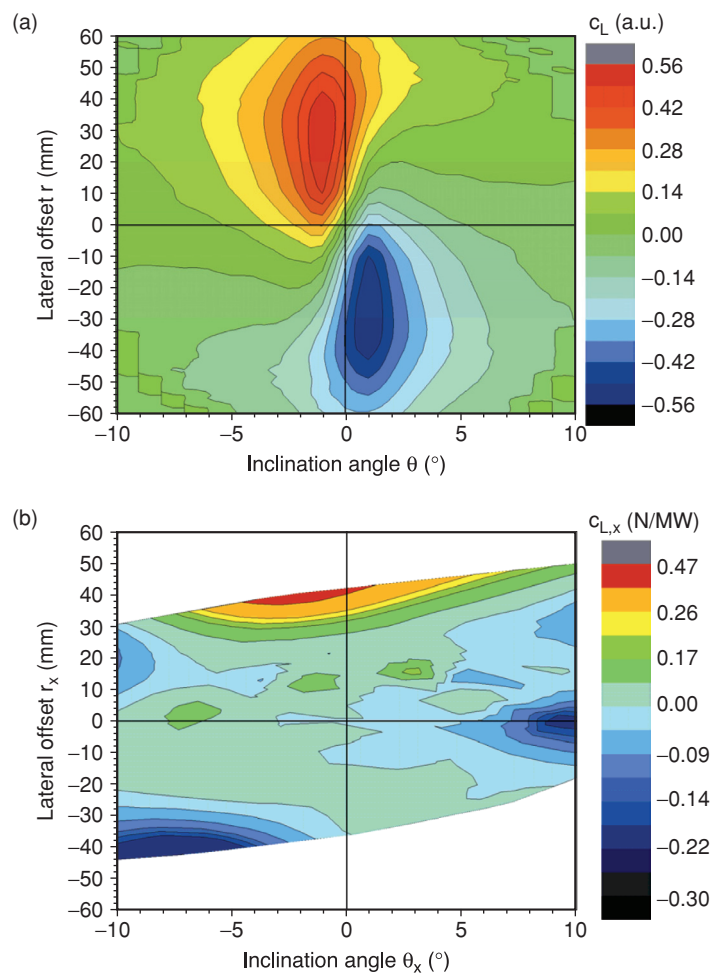


Figure 7. Dependency of the rotational momentum on lateral offset and inclination angle of the lightcraft against the laser beam. Theoretical results from fluence distribution modeling (a) are compared with experimental data (b), cf. Section 3.3.

**Table 2. Variations of laser burst parameters corresponding to the Julia sets as depicted in Figure 8.**

Constant Parameter	Julia Set	Pulse Energy [J]	Repetition rate [Hz]	Average Power [kW]
<b>Repetition rate</b>	b)	69.5	<b>36</b>	2.5
	c)*	139	<b>36</b>	5
	d)	278	<b>36</b>	10
<b>Pulse energy</b>	d)	<b>139</b>	18	2.5
	c)*	<b>139</b>	36	5
	b)	<b>139</b>	72	10
<b>Average Power</b>	a)	69.5	72	<b>5</b>
	c)*	139	36	<b>5</b>
	e)	278	18	<b>5</b>

\*Julia set c) corresponds to the laser burst parameters of the experiment described in Section 3.

Since we assumed that the imparted differential impulse should be proportional to the fluence, it can be easily seen from Equation 14 that varying the average laser power  $P$  by a factor  $\kappa$  at constant pulse energy leads to the same Julia set as varying  $P$  by  $\kappa^{-1}$  at constant repetition rate. Furthermore, for a given  $P$  the most stable launch conditions appear to be created with low pulse energy and a high repetition rate. In that case, the corrective effect of lateral and rotational momentum seems to be the most pronounced since the free flight times between the pulses are short and overcompensation by the dynamical system is less likely because of the low pulse energy.

Nevertheless, it should be pointed out that in this model inclination is only concerned with respect to the direction of lateral offset. A more realistic model, however, should also include the twist angle of the lightcraft against the offset direction.

### 5.3. Comparison with experimental data

In a laboratory experiment, the number of pulses is reasonably limited due to the laboratory ceiling and the field of view of the tracking instrument unless a hovering experiment is conducted. Moreover, in a practical application the number of beam-riding pulses is less interesting than the achievable flight altitude with respect to misalignment.

In an earlier experiment, we examined free flights of 10 laser pulses with varying laser burst parameters for three flights each. The alignment facilities were less elaborate and restricted to a HeNe laser for centering of the lightcraft and a 2D spirit level for horizontal alignment. The flight altitudes immediately before the 10<sup>th</sup> pulse were compared with model predictions.

For modeling of the flight altitude we calculated the temporal course of lateral offset and inclination angle during the flight depending on the initial misalignment of the lightcraft in a Julia set with the same parameters as in Section 5.2. In parallel, however, for each laser pulse we determined the coupling coefficient in  $z$ -direction depending on the actual misalignment during the flight from Equation 12. Neglecting frictional losses, this finally yields the predicted flight altitude that is depicted in Figure 8. The data are normalized on the flight altitude  $h_0$  that is expected for  $z = 0$  where losses due to lateral offset and inclination vanish. Figure 9 shows that the central, bright area enlarges with increasing repetition rate indicating less sensitivity to slight misalignment. The fractal patterns show some similarity with respect to the Julia sets depicted in Figure 8: The central zone of stability runs linearly through zero with a slight slope of around  $0.1^\circ/\text{mm}$  (inclination per offset). However, the branches around  $\pm 10 - 20$  mm offset with an inclination even exceeding  $\pm 10^\circ$  are not found in Figure 9. This may be attributed to the unequal definition of the Julia set, which is based on the generation of positive thrust in beam direction in Equation 15, but is restricted to a positive altitude and thus a positive  $c_{m,eff}$  in the latter case.

The agreement of the experimental data with the theoretical values significantly depends on the laser burst parameters, cf. Figure 10. The theoretical values of  $h_0$  have been taken from the calculation of the Julia sets that are shown in Figure 9. Since the means of alignment of the lightcraft at the launch position were limited in that specific experiment, we conclude that the deviation of the experimentally

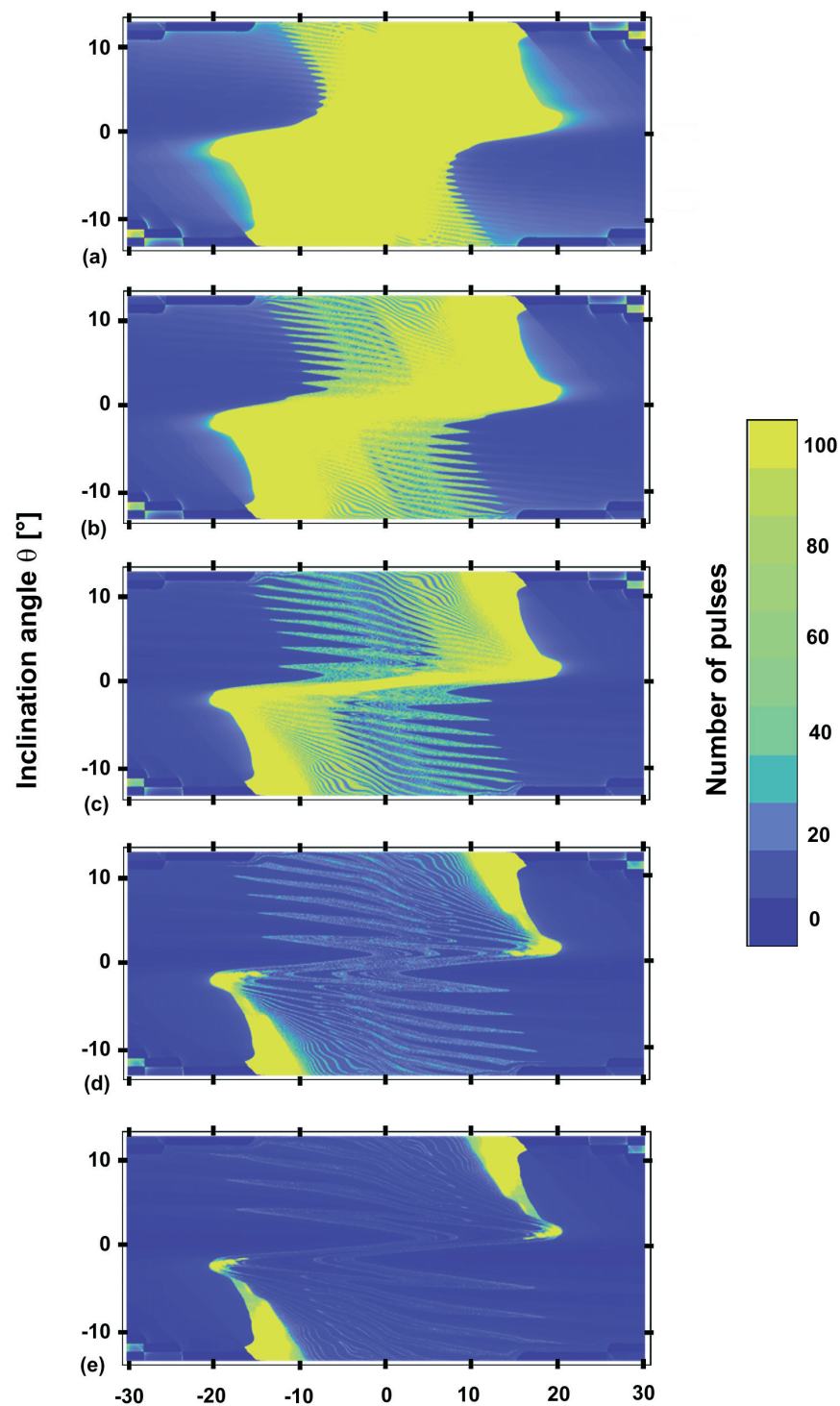


Figure 8. Visualization of the non-linear dynamics of a parabolic laser lightcraft as a Julia set. The pixel color indicates the number of pulses after which the lightcraft still stays within the laser beam. The laser burst parameters of the graphs are listed in Table 2.

found flight altitudes from  $h_0$  is mainly due to misalignment. In the experiment, this may lead to rather statistical results. Nevertheless, the agreement with the theoretical value increases with the repetition rate. This corresponds with the larger central bright area in Figure 9 for high repetition rates, which indicates a reduced dependence of the flight dynamics against initial misalignment. Hence, it turns out

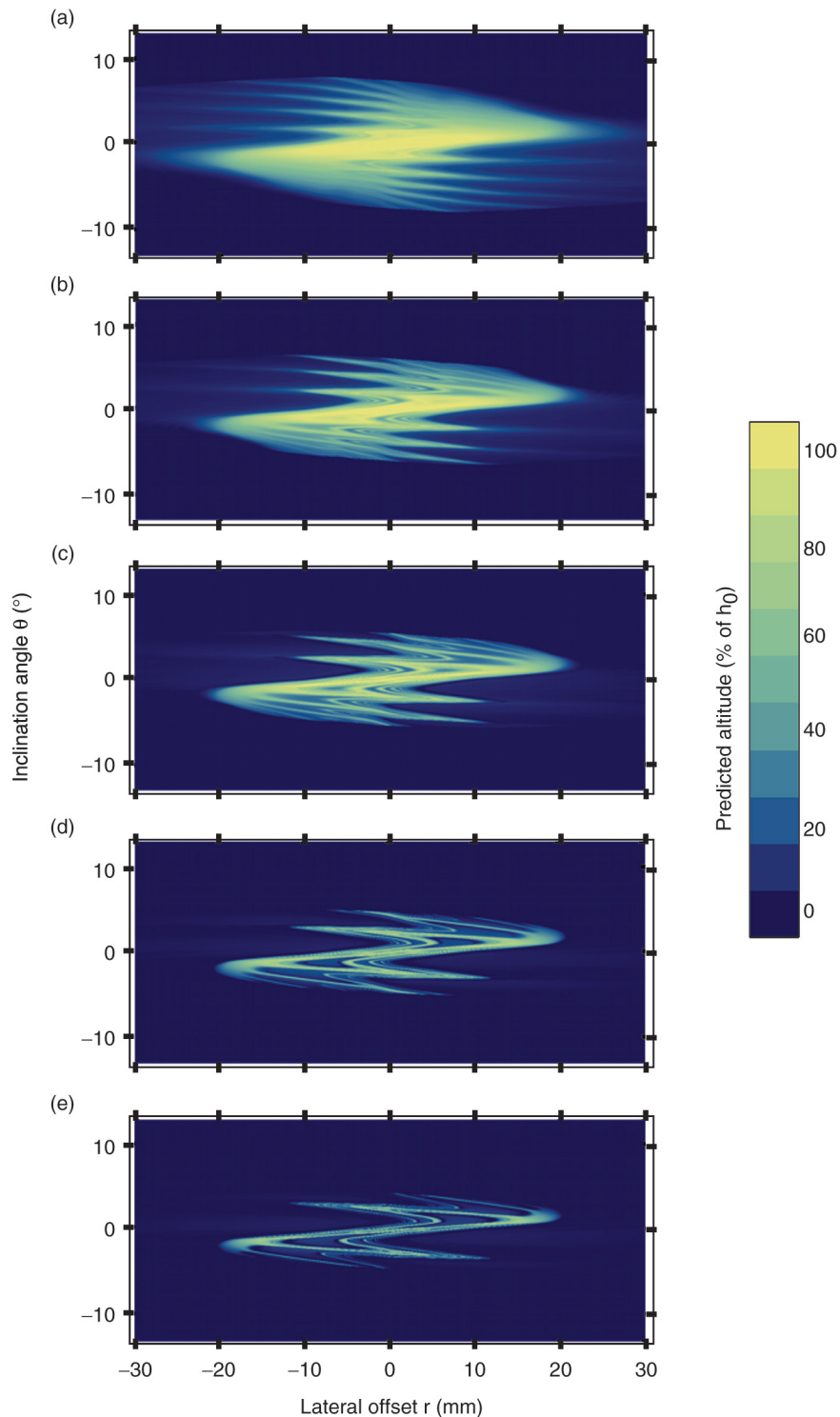


Figure 9. Predicted altitude (immediately before the 10<sup>th</sup> pulse) vs. initial offset and inclination angle of the lightcraft. Bright yellow color corresponds to maximum flight altitude  $h_0$  achieved with perfect alignment. Laser burst parameters are  $E = 135$  J with varying  $f_{rep}$ : 40.0 Hz (a), 28.6 Hz (b), 23.3 Hz (c), 18.6 Hz (d), and 16.1 Hz (e).

that a good accordance of experimental data with the theoretical value corresponds to a large zone of stability around the origin where the expected altitude differs not significantly from the optimum value (no offset or inclination). This was also observed under variation of pulse energy and laser burst variation under constant average power.

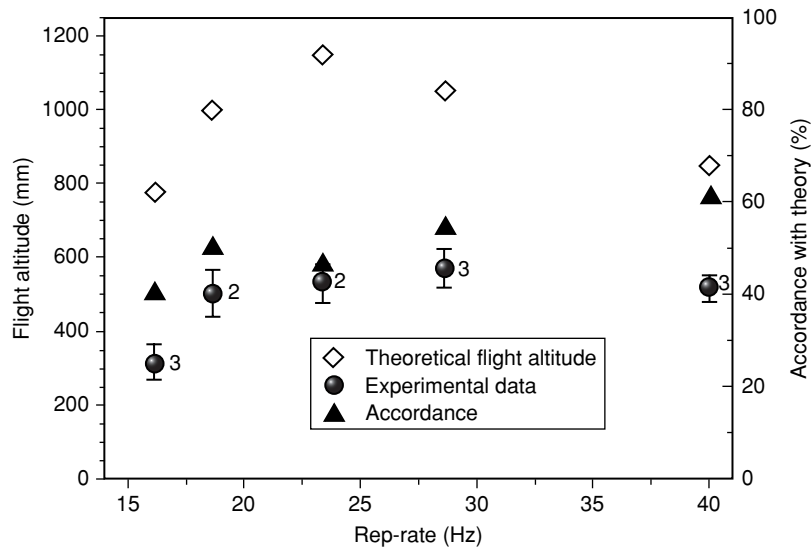


Figure 10. Comparison of flight altitudes in a laser burst immediately before the 10<sup>th</sup> pulse at a pulse energy of 135 J. The number of corresponding flights is given next to the data points. The impulse coupling coefficient,  $c_m = 306$  N/MW, was determined from single pulse experiments [14].

## 6. CONCLUSIONS

A reliable technology should be tolerant against slight misalignment, which is likely to occur during a launch mission. We found out that the parabolic lightcraft exhibits beam-riding properties that can be derived from free flight experiments. Experimental data on 5D momentum coupling show a fair accordance with model results derived from fluence calculations. However, a more rigorous model approach should consider the expansion of a spatially modified ring detonation with counterpressure acting on the parabolic geometry in a way similar to the calculations for a point explosion in [18]. Further experimental work will focus on hovering experiments with a fine adjustment of the laser burst to the lightcraft's weight in order to get more precise information on the impulse components and the flight stability [20].

Lateral and rotational force components causing reorientation of the lightcraft towards the laser beam depend non-linearly on offset and inclination angle. The complex dependency of the beam-riding abilities on 2D initial parameters and laser burst settings has been visualized by Julia sets. Further research will concentrate on the expansion of the corresponding parameter space.

## ACKNOWLEDGEMENTS

The authors want to thank Sebastian Walther, Frank-Uwe Holzschuh and Uli Nesper for their technical support. We thank Wolfgang O. Schall, John Sinko, and David Kenoyer for fruitful discussions. This work is dedicated to the memory of Horst-Dieter Scharring (1934-2009) who inspired me to explore the world of fractal images.

## REFERENCES

- [1] Askarian, G.A. and Moroz, E.M., Pressure produced at evaporating of matter under the beam of radiation, *Journal of the Experimental and Technical Physics*, Letters to Editor, 1962, 43(12), 2319–2321.
- [2] Kantrowitz, A., Propulsion to orbit by ground-based laser, *Astronautics & Aeronautics*, 1972, 10, 74–76.
- [3] Myrabo, L.N., World Record Flights of Beam-Riding Rocket Lightcraft: Demonstration of “Disruptive” Propulsion Technology, in: *37<sup>th</sup> AIAA/ASME/SAE/ASEE Joint Propulsion Conference, Paper AIAA 2001–379*.

- [4] Myrabo, L.N., Brief History of the Lightcraft Technology Demonstrator (LTD) Project, in: Pakhomov, A.V., ed., *First International Symposium on Beamed Energy Propulsion, AIP Conference Proceedings*, American Institute of Physics, Melville, New York, 2003, 664, 49–60.
- [5] Eckel, H.-A. and Schall, W.O., Concept for a Laser Propulsion Based Nanosat Launch System, in: Komurasaki, K., ed., *Proceedings of the Second International Symposium on Beamed Energy Propulsion, AIP Conference Proceedings*, American Institute of Physics, Melville, New York, 2004, 702, 263–273.
- [6] Bohn, W.L., Laser Propulsion – *Quo Vadis*, in: Pakhomov, A.V., ed., *Proceedings of the Fifth International Symposium on Beamed Energy Propulsion, AIP Conference Proceedings*, American Institute of Physics, Melville, New York, 2008, 997, 47–55.
- [7] Scharring, S., Eckel, H.-A., Trommer, J., Röser, H.-P., and Eigenbrod, C., Spaceborne Lightcraft Applications – An Experimental Approach, in: Pakhomov, A.V., ed., *Proceedings of the Fifth International Symposium on Beamed Energy Propulsion, AIP Conference Proceedings*, American Institute of Physics, Melville, New York, 2008, 997, 295–303.
- [8] Phipps, C.R., Luke, J.R., Helgeson, W., and Johnson, R., A ns-pulse Laser Microthruster, in: Komurasaki, K., Yabe, T., Uchida, Sh., and Sasoh, A., eds., *Proceedings of the Fourth International Symposium on Beamed Energy Propulsion, AIP Conference Proceedings*, American Institute of Physics, Melville, New York, 2006, 830, 235–246.
- [9] Phipps, C.R. et al, ORION: Clearing near-Earth Space Debris using a 20 kW, 530-nm, Earth-Based, Repetitively Pulsed Laser, *Laser and Particle Beams*, 1996, 14(1), 1–44.
- [10] Libeau, M.A., Myrabo, L.N., Filippelli, M., and McInerney, J., Combined Theoretical and Experimental Flight Dynamics Investigation of a Laser-Propelled Vehicle, in: Pakhomov, A.V., ed., *Proceedings of the First International Symposium on Beamed Energy Propulsion, AIP Conference Proceedings*, American Institute of Physics, Melville, New York, 2003, 664, 125–137.
- [11] Libeau, M. and Myrabo, L.N., Off-Axis and Angular Impulse Measurements on a Lightcraft Engine, in: Pakhomov, A. V. and Myrabo, L. N., eds., *Proceedings of the Third International Symposium on Beamed Energy Propulsion, AIP Conference Proceedings*, American Institute of Physics, Melville, New York, 2005, 766, 166–177.
- [12] Kenoyer, D.A., Anderson, K.S., and Myrabo, L.N., Validation And Calibration Of A 6-DOF Laser Propelled Lightcraft Flight Dynamics Model vs. Experimental Data, in: Pakhomov, A.V., ed., *Proceedings of the Fifth International Symposium on Beamed Energy Propulsion, AIP Conference Proceedings*, American Institute of Physics, Melville, New York, 2008, 997, 325–337.
- [13] Schall, W.O., Zeyfang, E., Riede, W., and Mayerhofer, W., Patent DE 100 17 343 C2 (7 Apr 2000) (in German) and US 2002/0047673 A1 (6 Apr 2001).
- [14] Scharring, S., Hoffmann, D., Eckel, H.-A., and Röser, H.-P., Stabilization and steering of a parabolic laser thermal thruster with an ignition device, *Acta Astronautica*, 2009, 65, 1599–1615.
- [15] Schall, W.O., Eckel, H.-A., Mayerhofer, W., Riede, W., and Zeyfang, E., Comparative lightcraft impulse measurements, in: Phipps, C.R., ed., *Proceedings of the Conference on High Power Laser Ablation IV, Proceedings of SPIE*, 2002, 4760, 908–917.
- [16] Mayerhofer, W., Zeyfang, E., and Riede, W., Design data of a repetitively pulsed 50 kW Multigas Laser and recent experimental results, *XII International Symposium on Gas Flow and Chemical Lasers and High-Power Laser Conference, Proceedings of SPIE*, 1998, 3574, 644–648.
- [17] Scharring, S., Sinko, J., Sasoh, A., Eckel, H.-A., and Röser, H.-P., Experimental determination of the impulse coupling coefficient – Standardization issues, *International Journal of Aerospace Innovations*, 2011, 3(1), 33–43.
- [18] Ageev, V.P., Barchukov, A.I., Bunkin, F.V., Konov, V.I., Prokhorov, A.M., Silenok, A.S., and Chapliev, N.I., Laser air-breathing jet engine, *Soviet Journal of Quantum Electronics*, 1977, 7(12), 1430–1437.

- [19] Sinko, J. (private communication, 21 Feb 2008).
- [20] Scharring, S., Eckel, H.-A., and Röser, H.-P., High speed analysis of free flights with a parabolic thruster, in: Phipps, C.R., Komurasaki, K., and Sinko, J.E., eds., *Proceedings of the Sixth International Symposium on Beamed Energy Propulsion, AIP Conference Proceedings*, American Institute of Physics, Melville, New York, 2010, 1230, 77–88.
- [21] Scharring, S., Eckel, H.-A., and Röser, H.-P., Flight Analysis of a Parabolic Lightcraft – Ground-based Launch, in: Pakhomov, A.V., ed., *Proceedings of the Fifth International Symposium on Beamed Energy Propulsion, AIP Conference Proceedings*, American Institute of Physics, Melville, New York, 2008, 997, 304–315.
- [22] Barnsley, M., *Fractals Everywhere*, Academic Press Inc., San Diego, 1988, 248–268.